Correspondence to:
E. I. Biao,
biaoeliezer@yahoo.fr

Impact of Stratospheric Aerosol Geoengineering on Extreme Precipitation and Temperature Indices in West Africa Using GLENS Simulations

E. A. Alamou[1,2], J. E. Zandagba[1,2], E. I. Biao[1,2] , E. Obada[1,2], C. Y. Da-Allada[2,3] , F. K. Bonou[3] , Y. Pomalegni[3], E. Baloitcha[3], S. Tilmes[4] , and P. J. Irvine[5]

[1]Laboratory of Applied Hydrology, National Water Institute, University of Abomey-Calavi, Godomey, Benin, [2]Laboratory of Geosciences, Environment and Applications, National University of Sciences, Technology, Engineering and Mathematics, Abomey, Benin, [3]International Chair in Mathematical Physics and Applications (ICMPA-UNESCO CHAIR), University of Abomey-Calavi, Godomey, Benin, [4]National Center for Atmospheric Research, Boulder, CO, USA, [5]Harvard John A. Paulson School of Engineering and Applied Sciences, Cambridge, MA, USA

Abstract This study assesses changes in extremes precipitation and temperature in West Africa under a high greenhouse gas scenario, that is, a representative concentration pathway 8.5, and under a scenario of stratospheric aerosol geoengineering (SAG) deployment using the NCAR Community Earth System Model version 1. We use results from the Geoengineering Large Ensemble simulations (GLENS), where SAG is deployed to keep global surface temperatures at present day values. This impact study evaluates changes in some of the extreme climate indices recommended by the Expert Team Monitoring on Climate Change Detection and Indices. The results indicate that SAG would effectively keep surface temperatures at present day-conditions across a range of indices compared to the control (CRTL) period, including Cold days, Cold nights and Cold Spell Duration Indicator which show no significant increase compared to the CRTL period. Regarding the extremes precipitation, GLENS shows mostly a statistically significant increase in annual precipitation and statistically significant decrease in the number of heavy and very heavy precipitation events relative to the CRTL period in some regions of Gulf of Guinea. In the Sahel, we notice a mix of statistically significant increase and decrease in Max 1-day and Max 5-days precipitation amount relative to the CRTL period at the end of the 21st century when large amounts of SAG has been applied. The changes in extreme precipitation indices are linked to changes in Atlantic Multidecadal Oscillation, NINO3.4 and Indian Ocean Dipole and these changes in extreme precipitation are driven by change in near surface specific humidty and atmospheric circulation.

1. Introduction

Geoengineering, which covers carbon removal as well as sunlight reflection, is discussed in recent literature as a potential option for reducing the most dangerous changes to Earth's climate as a result of large greenhouse gas increases (Launder & Thompson, 2009). According to Tilmes et al. (2013), one of the proposals to "buy some time" while mitigation scenarios are aggressively ramped up, considers the reduction of incoming shortwave radiation, called solar radiation management (SRM). SRM is expected to play a significant role in mitigating global temperature increases; however, the relative impacts and risks of these engineering practices need to be closely examined. Geoengineering using sulfur injections into the stratosphere has been proposed as a method to deliberately counteract global warming as a result of anthropogenic climate change (Crutzen, 2006). Stratospheric aerosol geoengineering (SAG) is the proposed SRM method that has received the most sustained attention.

In fact, past modeling studies have examined the impacts of SRM on climate and shown that uniform reductions in the solar constant can roughly compensate for globally averaged surface warming from a doubling and quadrupling of CO_2 concentrations (Caldeira & Wood, 2008; Govindasamy & Caldeira, 2000; Govindasamy et al., 2003; Kravitz, Caldeira, et al., 2013). Similar studies have also observed that if global-mean temperature is restored there would be a decrease in the pole-to-equator temperature gradient relative to a case without elevated CO_2 and that there would be a slowdown of the hydrologic cycle, including a decrease in global mean, annual mean precipitation (Ammann et al., 2010; Bala et al., 2008; Kalidindi et al., 2015; Kravitz, Rasch, et al., 2013; McCusker et al., 2012; Niemeier et al., 2013; Ricke et al., 2010; Schmidt et al., 2012; Tilmes et al., 2013).

In contrast to earlier studies, the use of the SAG in the Geoengineering Large Ensemble simulations (GLENS) have not only targeted global surface temperature but also the interhemispheric temperature gradient, and the equator-to-pole temperature gradient. These goals were achieved using a feedback algorithm to identify annual sulfur dioxide injections at 4 locations (i.e., at ∼5 km above the tropopause, namely at 30°N, 30°S, 15°N, and 15°S) into the stratosphere (Kravitz et al., 2017). The GLENS simulations that has been set up prescribed greenhouse gas forcing concentrations following the representative concentration pathway 8.5 (RCP8.5, i.e., a high anthropogenic emission scenario). This setup requires steadily increasing sulfur injections for the geoengineering simulations to counteract the forcing of increasing greenhouse gases in order to keep the climate at 2020 conditions.

Despite the GLENS simulations performance at maintaining overall climate conditions, Simpson et al. (2019) has pointed to substantial regional precipitation changes for some regions, include a reduction in precipitation in the Indian summer monsoon, over much of Africa, Amazonia and southern Chile and a wintertime precipitation reduction over the Mediterranean. Several studies already evaluated changes in key climate extreme indices under SAG, that is, Curry et al. (2014) and Ji et al. (2018) at large scale; Pinto et al. (2020) in Africa. However, these earlier studies have neither explored local changes in West Africa nor elucidated the basic processes associated with West African rainfall variations.

Nevertheless, numerous studies found that oceanic forcing was the main driver of the Sahel and West Africa rainfall variability on interannual and decadal time scales. Most of them agree that SSTs is the main player in forcing rainfall variability in the southern part of West Africa (Camberlin et al., 2001; Chang et al., 2000; Nicholson, 2013; Vizy & Cook, 2001). Giannini et al. (2003) confirmed that West African monsoon variability at time scales from interannual to multidecadal is mainly driven by global ocean sea surface temperature (SST) anomalies. Other studies investigated the influence of ocean basins on extreme precipitation. Gao et al. (2017) showed that the Indian Ocean Dipole (IOD), El Niño-Southern Oscillation and Atlantic Multidecadal Oscillation (AMO) all have strong impacts on monsoon and extreme precipitation in China, especially during the 1990s, which is generally consistent with the abrupt shifts in precipitation regimes around this period. Recently, Atiah et al. (2020) tried to understand the link between 10 rainfall indices over Ghana and SST in different regions. Their results revealed very few significant correlation between the SST anomalies over oceanic basins, and the consecutive dry days (CDD), consecutive wet days (CWD), max-1 day precipitation amount (RX1day), number of very heavy precipitation (RX5day) and simple daily intensity index (SDII) thus indicating the frequency of daily indices over the region are probably more driven by seasonal scale variability than interannual variability in SST over the ocean basins. Generally, SST anomalies at the Pacific and Indian Oceans had negative correlations with wet rainfall indices, whereas the Atlantic SST had positive correlations with wet indices over Ghana.

The present study focuses on West Africa, which is known to be particularly vulnerable to climate change due to high climate variability, high reliance on rain-fed agriculture, and limited economic and institutional capacity to respond to climate variability and change (Sultan & Gaetani, 2016). The objective is to (a) assess changes in extreme precipitation and temperature in West Africa under a high greenhouse gas scenario and using SAG and to (b) identify the link between SST anomalies and extreme precipitation. We focus on a period where very large amount of SAG has been applied (2070–2090) to counter a high forcing scenario in order to identify more significant changes. Here, we investigate some of the climate extreme indices recommended by the Expert Team Monitoring on Climate Change Detection and Indices (ETCCDI) (Zhang et al., 2011). The indices describe particular characteristics of extremes, including frequency, amplitude and persistence.

2. Materials and Methods

2.1. Study Area

The West African region is situated between 4°N and 28°N latitude and −17°W and 16°E longitude (Figure 1), covering a total area of 6 million km² (one fifth of Africa) with the Gulf of Guinea as its southern boundary (Onojeghuo et al., 2017). West Africa's climate is controlled by the interaction of several air masses (the northerly and southerly winds, the jets, the waves, the heat low, etc.) (Sylla et al., 2013), the influence of which varies throughout the year with the north-south movement of the Intertropical Convergence Zone (ITCZ). Hot, dry continental air masses originating from the high pressure system above the Sahara Desert give rise to dusty
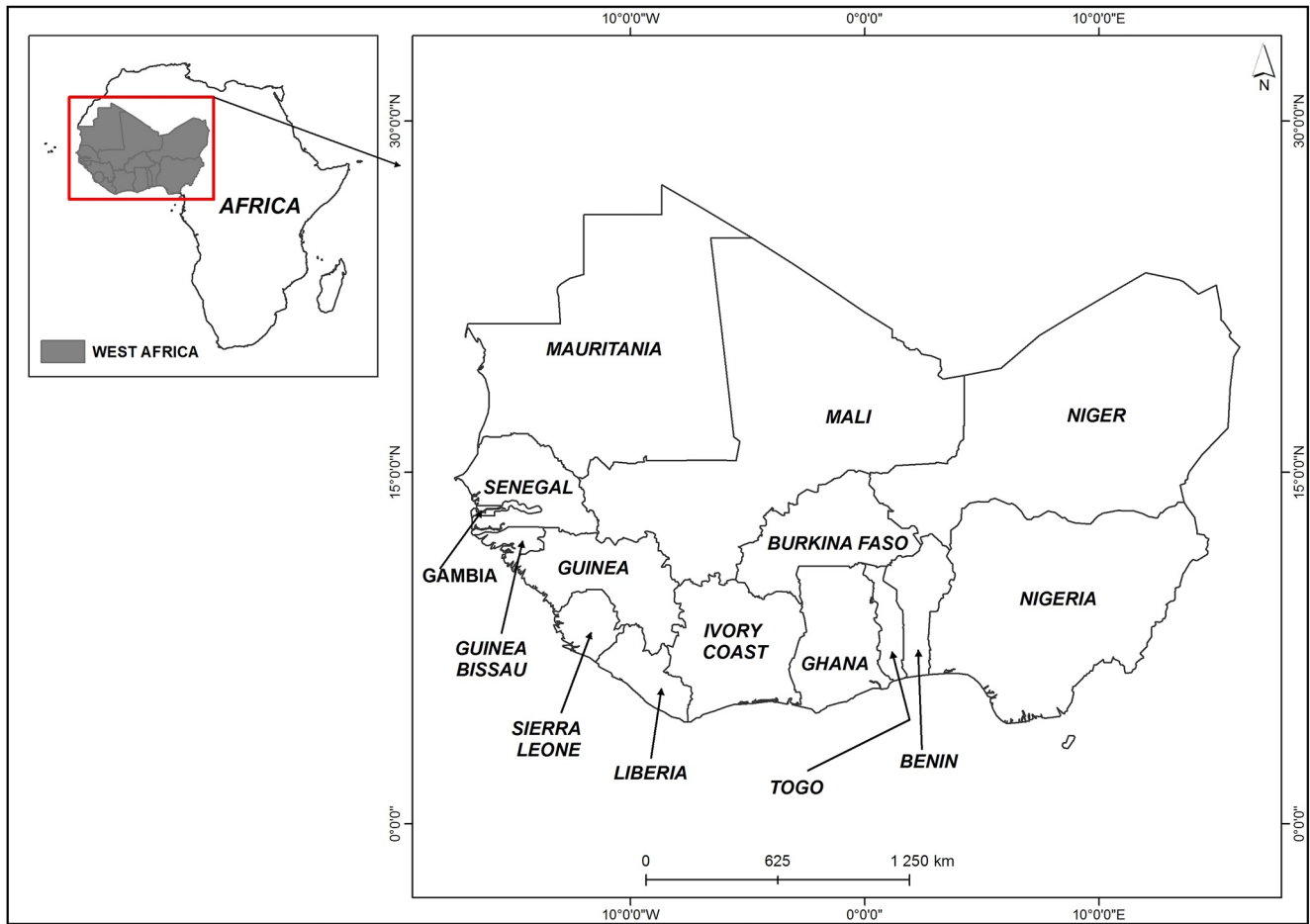
Figure 1. West Africa region.

Harmattan winds over most of West Africa from November to February. In summer, moist equatorial air masses originating over the Atlantic Ocean bring annual monsoon rains (Nicholson, 2013). Mean annual minimum and maximum temperatures are comprised between 16 and 20°C for the minimum and 27 and 35°C for the maximum depending on the proximity of the ocean (Ly et al., 2013).

2.2. Data

Data used in this study consist of the combined observations and satellite data set of the CPC Global PRCP V1.0 (https://www.esrl.noaa.gov/psd/data/gridded/data.cpc.globalprecip.html), CPC Global TEMP V1.0 (https://www.esrl.noaa.gov/psd/data/gridded/data.cpc.globaltemp.html) and model data from the GLENS project (precipitation, temperatures and SST) (Tilmes, Richter, Kravitz, et al., 2018; Tilmes, Richter, Mills, et al., 2018). The GLENS simulations use prescribed greenhouse gas forcing concentrations following the RCP8.5 (i.e., a high forcing scenario) (Tilmes, Richter, Kravitz, et al., 2018; Tilmes, Richter, Mills, et al., 2018). The Stratospheric Aerosol GLENS project is a 20-member ensemble of stratospheric sulfate aerosol geoengineering simulations between 2020 and 2099 and a 20-member ensemble of CRTL simulations over a reference period between 2010 and 2030 using the NCAR Community Earth System Model with the Whole Atmosphere Community Climate Model (WACCM) as its atmospheric component (CESM1 WACCM) described in Mills et al. (2017) (Table 1). However, in this study, we are using three ensemble member for the CRTL, RCP8.5, and the SAG simulations (GLENS).

Table 1
Summary of Available Model Simulations Used in This Study

Simulation	Years	Ensemble member
Control	2010–2030	3 (001–003)
RCP8.5	2070–2090	3 (001–003)
GLENS	2070–2090	3 (001–003)

The observed precipitation and temperature data are daily data with $0.5 \times 0.5°$ spatial resolution. Model simulations consist of: historical simulations (1980–2010), CRTL simulations (2010–2030), RCP8.5 simulations (2070–2090) and GLENS simulations (2070–2090). Details about the data and simulations used in this study can be found in Kravitz et al. (2017), Tilmes, Richter, Kravitz, et al. (2018), and Tilmes, Richter, Mills, et al. (2018). These data are from a grid of $0.95 \times 1.25°$ and the Inter-Sectoral Impact Model Intercomparison Project (ISIMIP) bias correction method (Hempel et al., 2013) has been applied to bias correct data from a grid of $0.5 \times 0.5°$ spatial resolution.

This bias correction method preserves the long-term absolute (relative) trend of the simulated temperature or precipitation data. The method modifies the daily variability of the simulated data about their monthly means to match the observed daily variability. The monthly variability and mean are corrected only using a constant offset or multiplicative correction factor that corrects for long-term differences between the simulated and observed monthly mean data in the historical period. In this way the absolute or relative trend of the simulation data is preserved.

2.3. Methods

The work reported herein investigates the spatial patterns of extremes precipitation and temperature in West Africa region. In this study, we used 16 ETCCDI indices (Tables 2 and 3). The selected indices capture not only the intensity and duration of changes in temperature and precipitation, but also the frequency and length of heavy precipitation events. It also allows us to assess the spatial and temporal distribution of extreme events in the study area. All the investigated extremes climate indices are calculated from daily precipitation, maximum and minimum temperatures. These indices are computed on annual basis.

According to Wörner et al. (2019), applying bias correction on climate model data prior to the use seems necessary at local scale. Bias correction could remove some errors in climate models output. Bias correction addresses biases in model results that are the result of the way physical processes are captured in the original climate models, their boundary and initial conditions and the effects of the numerical algorithms used for solving the partial differential equations within the model. On the other hand, bias correction removed errors due to the large spatial scale of grid cells of models that doesn't take into account local climate specificity. These can be considered fundamental sources of bias that bias correction accounts for, but which do not necessarily make results more accurate or precise (Razavi et al., 2016). The bias correction of this study's simulations (historical, RCP8.5 and GLENS) has been done using CPC Global PRCP V1.0 for precipitation and CPC Global TEMP V1.0 for temperature and by applying ISIMIP method (Hempel et al., 2013). The data used for bias correction has been extracted by interpolation at a grid of $0.5 \times 0.5°$ that corresponds to the grid of CPC Global PRCP/TEMP. This bias correction method uses quantile mapping method designed to (a) robustly adjust biases in all percentiles of a distribution and (b) preserve trends in these percentiles (Hempel et al., 2013). It was designed to be applied to climate variables such as those used in the ETCCDI indices applied here. To evaluate the bias correction method

Table 2
Temperature Indices Summary

Common name	Indices	Description	Units
Cool nights	TN10p	Number of days when TN (daily minimum temperature) < 10th percentile of the control period	days
Warm nights	TN90p	Number of days when TN > 90th percentile of the control period	days
Tropical nights	TR	Annual count of days when TN > 20°C	days
Summer days	SU	Annual count of days when TX (daily maximum temperature) > 25°C	days
Warm days	TX90p	Number of days when TX > 90th percentile of the control period	days
Cool days	TX10p	Number of days when TX < 10th percentile of the control period	days
Cold spell duration indicator	CSDI	Annual count of days with at least 6 consecutive days when TN < 10th percentile of the control period	days
Warm spell duration indicator	WSDI	Annual count of days with at least 6 consecutive days when TX > 90th percentile of the control period	days

Table 3
Rainfall Indices Summary

Common name	Indices	Description	Units
Consecutive dry days	CDD	Maximum number of consecutive days with RR < 1 mm	days
Consecutive wet days	CWD	Maximum number of consecutive days with RR ≥ 1 mm	days
Simple daily intensity index	SDII	Annual total precipitation divided by the number of wet days (defined as PRCP ≥ 1.0 mm) in the year	mm/days
Max 1-day precipitation amount	RX1day	Annual maximum 1-day precipitation	mm
Max 5-day precipitation amount	RX5day	Annual maximum consecutive 5-day precipitation	mm
Number of heavy precipitation	R10	Annual count of days when PRCP ≥ 10 mm	days
Number of very heavy precipitation	R20	Annual count of days when PRCP ≥ 20 mm	days
Annual precipitation	P annual	Annual precipitation	mm

on the extreme climate indices, two performances criteria are used: the root mean square error (RMSE) and the mean absolute error (MAE).

To assess the impact of SAG on extreme precipitation and temperature indices, the difference between GLENS simulations and CRTL simulations have been computed. The spatial pattern of this difference allowed one to contrast changes in the future with or without geoengineering compared to present day, while following a high concentration pathway.

To quantify these changes, the difference between the mean of each investigated extreme precipitation and temperature indices derived from GLENS and CRTL simulations were calculated as follows:

$$\text{Changes} = X_{\text{future}} - X_{\text{control}} \tag{1}$$

where X_{future} represents the bias corrected projected extreme precipitation or temperature indices from the RCP8.5 and GLENS simulations over the period 2070–2090, and X_{control} represents the bias corrected RCP8.5 simulations over the period 2010–2030. Sylla et al. (2016) showed that the largest and more extended changes covering almost all West Africa are found by the end of the 21st Century and for the RCP8.5 scenario. This is the reason why this study focuses on the time period 2070–2090 for the assessment of the impact of SAG.

The Student *t*-test is used to determine whether there is a significant difference between the means of X_{future} and X_{control}.

In order to investigate the link between projected SST and extreme precipitation indices, Granger causality (Granger, 1969) test at 95% confidence level was computed. Granger test is a statistical test to find causality between two variables. The AMO index is a basin-scale mode of observed multidecadal climate variability which describes the average SST in the north of Atlantic (0°–70°N and 75–7.5 W) (Enfield et al., 2001). The NINO3.4 index is the average SST anomalies in the NINO3.4 region (5°N to 5°S, from 170°W to 120°W) (Barnston & Tippett, 2013). The IOD is a coupled ocean-atmosphere phenomenon occurring in Indian Ocean (Diatta & Fink, 2014) which describes the SST anomalous difference between the western parts of the equatorial Indian Ocean (50°–70°E and 10°S–10°N) and the south eastern equatorial Indian Ocean (90°–110°E and 10°S–0°N) (Vinayachandran et al., 2002). For Global mean SST anomalies, we aggregated the monthly SST into annual SST. Then we computed the annual mean of all gridded SST to have a time series of global mean SST. Finally, we calculated the anomalies these time series. For each investigated SST indices (AMO, NINO3.4, and IOD), we extracted SST in the windows of each indices and computed their anomalies following the same approach as for global mean SST anomalies. Finally, we computed Granger causality between each time series of SST indices and gridded extreme precipitation indices using Granger causality test (Granger, 1969).

To investigate the mechanism of changes in extreme precipitation under GLENS, we followed the approaches used by Da-Allada et al. (2020). They decomposed precipitation changes into their thermodynamic component (driven by changes in specific humidity), dynamic component (driven by changes in the tropical circulation), and nonlinear cross component (driven by both changes in specific humidity and circulation, i.e., negligible). In this study, we investigate changes in near surface specific humidity and 957 hPa wind fields to explain changes in extreme precipitation indices in West Africa under GLENS.
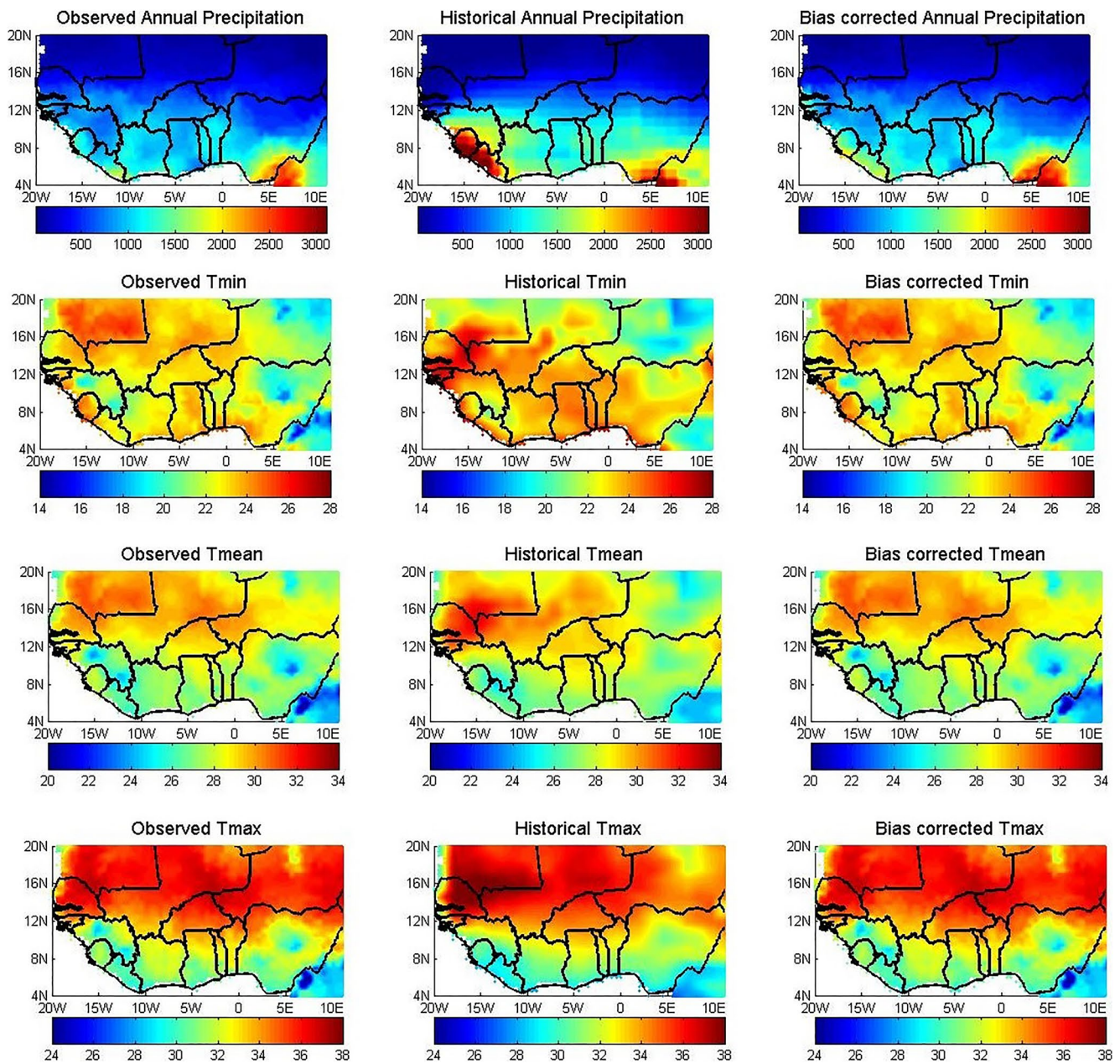
Figure 2. Inter-Sectoral Impact Model Intercomparison Project bias correction results for the precipitation (mm) and temperature (°C) for the period 1980–2010. The first column shows the observed data, the second column shows the non-corrected model data (historical data) and the third column shows the corrected model data (bias corrected data).

3. Results

3.1. Evaluation of ISIMIP Bias Correction Method on Precipitation and Temperature

The comparison between satellites precipitation (temperature) from CPC Global PRCP V1.0 (CPC Global TEMP V1.0) and historical GLENS precipitation (temperature) data show a significant bias in climate model data. When applying this data to calculate extremes climate indices, substantial differences were found between raw historical GLENS simulations and observed data. After applying the ISIMIP bias correction method, the large differences between observations data and historical GLENS simulations were reduced. Figure 2 shows the results of the application of the bias correction method for precipitation and temperature. It can be seen from this figure that the bias corrected data are closer to the observed data than the historical GLENS data. Table 4 shows the

Table 4
Performance Statistics Comparing Observation, Raw Historical and Bias Corrected Precipitation and Temperature Data

	Annual precipitation (mm)		T_{mean} (°C)		T_{min} (°C)		T_{max} (°C)	
	Raw	Corrected	Raw	Corrected	Raw	Corrected	Raw	Corrected
RMSE	451.65	119.11	1.11	0.01	1.74	0.1	1.20	0.02
MAE	232.96	58.33	0.75	0.02	1.27	0.05	0.80	0.02

performance statistics of the bias correction method using the RMSE and the MAE. The bias correction method has almost eliminated the errors in the surface air temperature metrics and reduced the error in precipitation substantially. These results imply that bias corrected data can be used to access the impact of SAG on West African future precipitation and temperature.

3.2. Changes in Extreme Temperature Indices Under SAG

3.2.1. Changes in Minimum, Maximum, and Mean Temperature

Figure 3 shows changes in minimum, maximum, and mean temperatures over the period 2070–2090 under RCP8.5 and GLENS simulations compared to the CRTL period 2010–2030 (CTRL). Under RCP8.5 scenario, West Africa would experience a statistically significant increase in minimum, maximum and mean temperature. The increase in minimum, maximum and mean temperature ranges between 1°C and 2°C in the Gulf of Guinea, while this increase is ranging between 3°C and 4°C in the Sahel region. These results are in line with Sylla et al. (2016) who found that, at the end of the century, possible warming over West Africa ranges from 1.5°C to 6.5°C, with the Sahel experiencing the largest changes. Under the GLENS scenario, a slight statistically significant increase in minimum temperature (between 0.5°C and 1°C) is simulated in some of the Sahelian region (between 12°N–20°N), while a statistically significant decrease (between 0°C and 1.5°C) is found in Gulf of Guinea region. For the maximum and mean temperature, a slight decrease (between 0°C and 0.5°C) is observed in West Africa. In general, the GLENS simulations reduce the changes in minimum, maximum and mean temperatures compared to the RCP8.5 scenarios over the period 2070–2090.

#### 3.2.2. Changes in Cold Extremes Indices (TX10p, TN10p, CSDI)

The changes in cold extremes relative to the CRTL period under RCP8.5 and GLENS simulations are shown in Figure 4. Under RCP8.5 scenario, by the end of the 21st century, most of West Africa countries would experience a statistically significant decrease (ranging between 0 and 40 days) in cool days (TX10p) and cool nights (TN10p) compared to the CRTL period. However, the decrease (ranging between 0 and 5 days) in cold spell duration indicator is less pronounced in comparison with TX10p and TN10p.

GLENS show a mix of non statistically significant increase (ranging from 0 to 22 days) and a significant decrease (ranging from 0 to 6 days) in TX10p. Regarding TN10p, a decrease (up to 32 days) is simulated in West Africa, except in Nigeria, northern Senegal and Mauritania where an increase of about 50 days is observed. A slight decrease (between 0 and 2 days) in CSDI is simulated in the study area, except in southern Nigeria, northern Senegal, and southern Mauritania where a slight increase of about 6 days is calcualted. These results indicate an increase in cold extreme indices under GLENS compared to the results obtained with RCP8.5 scenario.

#### 3.2.3. Changes in Hot Extremes Indices (TX90p, TN90p, TR, SU, WSDI)

Figure 5 depicts the changes in hot extremes indices relative to the CRTL period under RCP8.5 and GLENS simulations. From this figure it can be seen that West Africa would experience statistically significant increase in all of the investigated hot extremes indices under RCP8.5 scenario compared to the CRTL period. These increases in hot extremes indices are respectively consistent with the increase in maximum temperature for warm days (TX90p), warm spell duration indicator (WSDI), summer days (SU) and in minimum temperature for warm nights (TN90p), tropical nights (TR). TX90p and TN90p increase respectively by about 0–363 days and 40–359 days. Statistically significant increases in TR (up to 292 days), SU (up to 146 days) and WSDI (between 0 and 14 days) are simulated in most of West Africa countries under RCP8.5 scenario relative to the CRTL period.
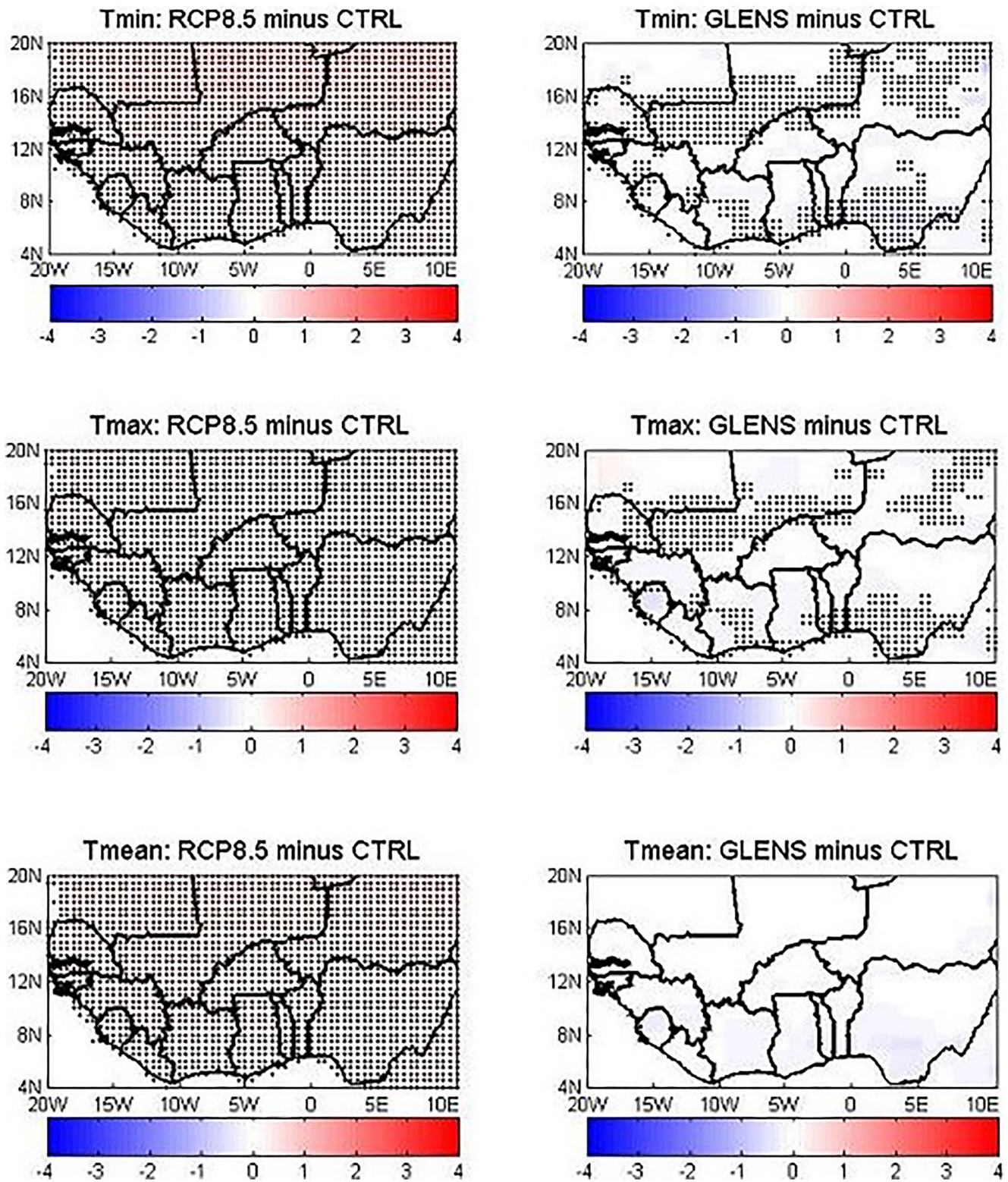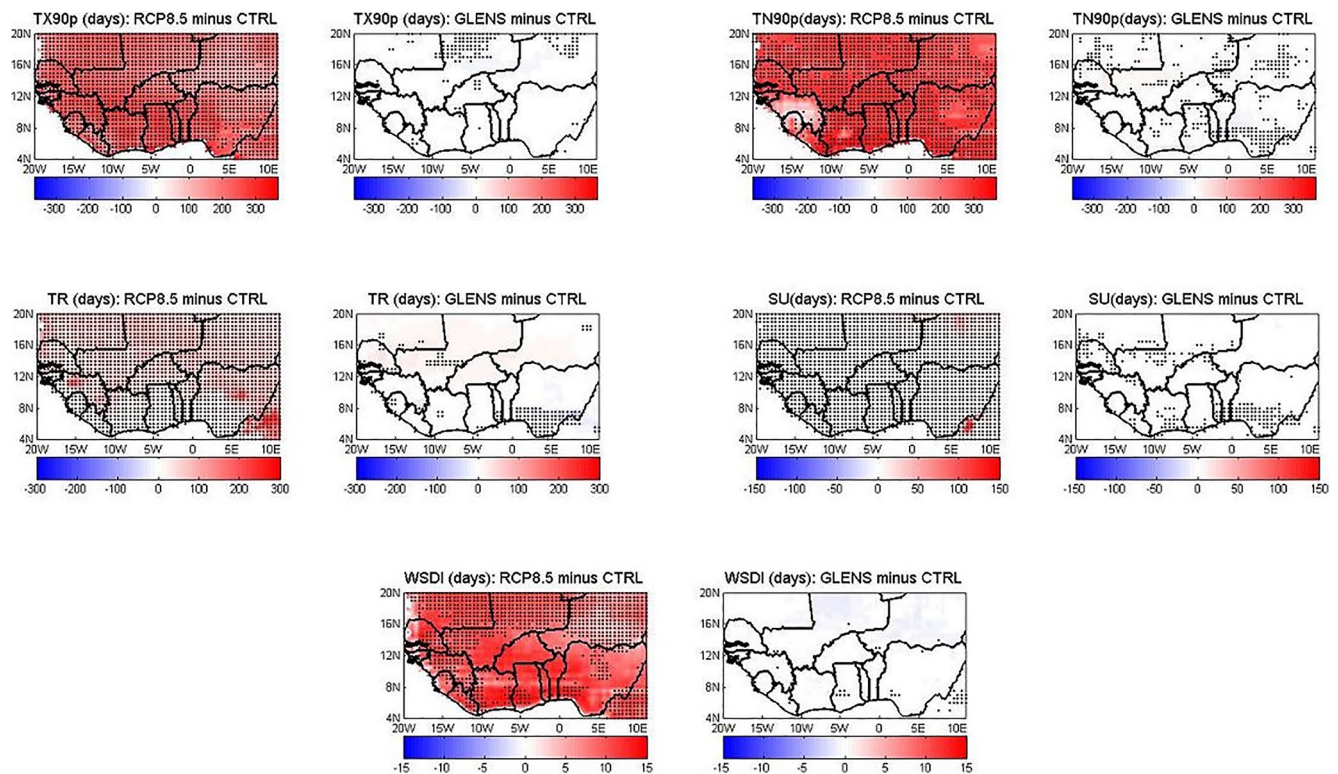
Figure 3. Changes in minimum (Line 1), maximum (Line 2), and mean (Line 3) Temperature (°C) over 2070–2090 compared to the control period (2010–2030) under representative concentration pathway 8.5 and Geoengineering Large Ensemble simulations. Hatching indicates regions where changes are significant at the 95% confidence level.
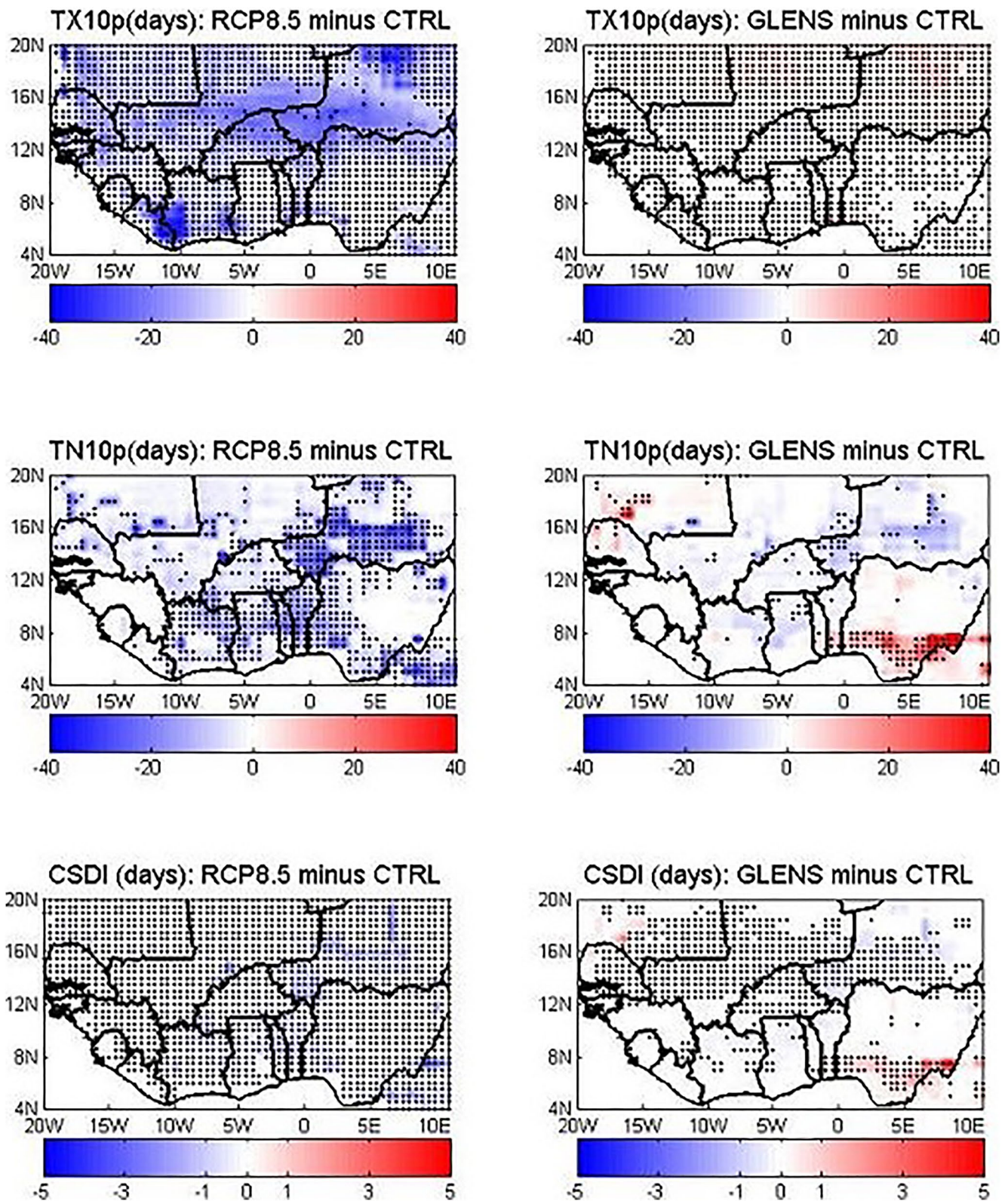
Figure 4. Changes in number of cool days (TX10p) (Line 1), number of cool nights (Tn10p) (Line 2), and in the Cold spell duration indicator (Line 3) compared to the control period (2010–2030) under representative concentration pathway 8.5 and Geoengineering Large Ensemble simulations. Hatching indicates regions where changes are statistically significant at the 95% confidence level.

Figure 5. Changes in warm days (TX90p), warm nights (Tn90p) (Line 1), Tropical nights, summer days (Line 2), and warm spell duration indicator (Line 3) compared to the control period (2010–2030) under representative concentration pathway 8.5 and Geoengineering Large Ensemble simulations. Hatching indicates regions where changes are statistically significant at the 95% confidence level.

Under GLENS simulations, all of the investigated hot extremes indices decrease slightly compared to the CRTL period, except for TR where a slight statistically significant increase (ranging between 0 and 50 days) is simulated in Sahel region. As shown in Figure 3, there is a statistically significant decrease in minimum temperatures in this region which can also be seen for TR and warm nights here. Meanwhile, the spatial pattern of warm days, SU and warm spell duration are consistent with maximum temperature.

In general, the results indicate that SAG reduces the hot extremes temperature indices compared to the results obtained with RCP8.5 scenario.

### 3.3. Changes in Extreme Precipitation Indices Under SAG

3.3.1. Changes in Annual Precipitation

Figure 6 shows changes in annual precipitation under RCP8.5 and GLENS simulations compared to the CRTL period. Under RCP8.5 and GLENS scenarios it is observed a statistically significant increase in annual precipitation in the Gulf of Guinea regions and some of Sahel regions (Burkina Faso, southern Mali, and west-southern Niger), except in southern Nigeria where a statistically significant decrease is noticed. In the Sahelian region, a slight statistically significant increase change (between 0 and 1 mm/days) appears under RCP8.5 scenario, except in Mauritania and Senegal. Under GLENS simulations, a slight decrease in annual precipitation is found in the Sahel. GLENS mostly reduce the increase in precipitation that is shown under RCP8.5 scenario for many regions.

3.3.2. Changes in Precipitation Intensity Indices (RX1day, RX5day, SDII)

Figure 7 shows changes in RX1day, RX5day, and SDII under RCP8.5 and GLENS scenarios relative to the CRTL period. Under RCP8.5 scenarios, RX1day and RX5day show a statistically significant increase, up to 50 mm in Guinea and Sierra Leone for RX1day and up to 100 mm in these countries for RX5days, in the region, except in Senegal, Mauritania, southern Nigeria, and north-east Niger where a statistically significant decrease of up to 50 mm is simulated. Under GLENS scenario, a statistically significant decrease in RX1day and RX5days of up
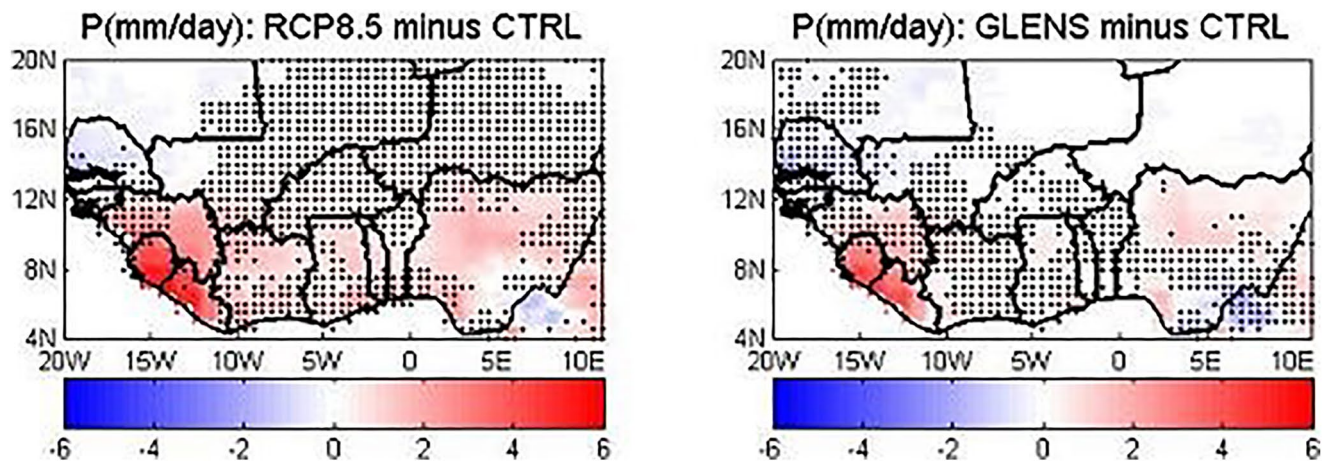
Figure 6. Changes in Annual Precipitation (mm/day) over the period 2070–2090 compared to the control period (2010–2030) under representative concentration pathway 8.5 and Geoengineering Large Ensemble simulations. Hatching indicates regions where changes are statistically significant at the 95% confidence level.

to 50 mm is simulated, although in Guinea, Sierra Leone, northern Ivory Coast, and northern Nigeria a slight non statistically significant increase (up to 20 mm) is found. Under both RCP8.5 and GLENS simulations, slight statistically significant decrease in SDII is simulated. However, under GLENS there are more regions with statistically significant changes, in particular in the Gulf of Guinea while less to the Sahelian region. From this analysis, it can be deduced that SAG reduces the precipitation intensity indices for some regions (Senegal, Mauritania) compared to the CRTL period, and reductions are slightly larger in GLENS than in RCP8.5 scenario. On the other hand, statistically significant increase in extreme precipitation obtained under RCP8.5 scenario over Guinea and Sierra Leone has been reduced under GLENS simulations.

### 3.3.3. Changes in Precipitation Frequency Indices (R10, R20, CWD, CDD)

Figure 8 shows changes in precipitation frequency indices under RCP8.5 and GLENS simulations compared to the CRTL period. Under RCP8.5 scenario it is observed a mix of slight statistically significant increase (ranging between 0 and 50 days) and a statistically significant decrease (up to 50 days) in the number of heavy precipitation (R10). Under GLENS simulations a statistically significant decrease (up to 50 days) in R10 is found in the study region, except in Guinea, Liberia and Sierra Leone where fewer statistically increase (ranging between 0 and 50 days) are found. These results look very similar to the changes in the number of very heavy (R20) precipitation days (not presented here).

Under both RCP8.5 and GLENS scenarios, no significant change in CWD is found in the Gulf of Guinea. Regarding the CDD, under RCP8.5 scenario, it is observed a decrease (ranging between 0 and 50 days) which is statistically significant in some areas, except in Senegal and Mauritania where no significant increase (up to 25 days) are simulated. Under GLENS simulations, a mix of slight non statistically significant decrease and increase (between −10 and 10 days) in CDD, except in Senegal and Mauritania where the increase in CDD can reach 50 days and in north-east Niger where the decrease can reach 40 days. It stems from this analysis that under SAG, CDD increases relative to RCP8.5 scenario.

### 3.4. Link Between SST and Extreme Precipitation Indices

Figure 9 shows the link between extreme precipitation indices and global mean SST under GLENS simulations over West Africa. The significant Granger causal relationship is indicated with hatching. Significant Granger causal relationship at 95% confidence level were found between global SST mean and R10, R20, RX1day. RX5day, CDD, CWD and SDII RX1day, RX5day, and SDII in most part of West Africa. The results from Granger causality tests support the important role of global SST mean in controlling extreme precipitation indices. However, in most part of Sahelian and Sahara regions, Granger causal relationship is not significant for all extreme indices like in golf coast area. These results indicate that the frequency of the extreme precipitation indices over Sahelian and Sahara regions is probably more driven by seasonal scale variability than interannual variability in SST over
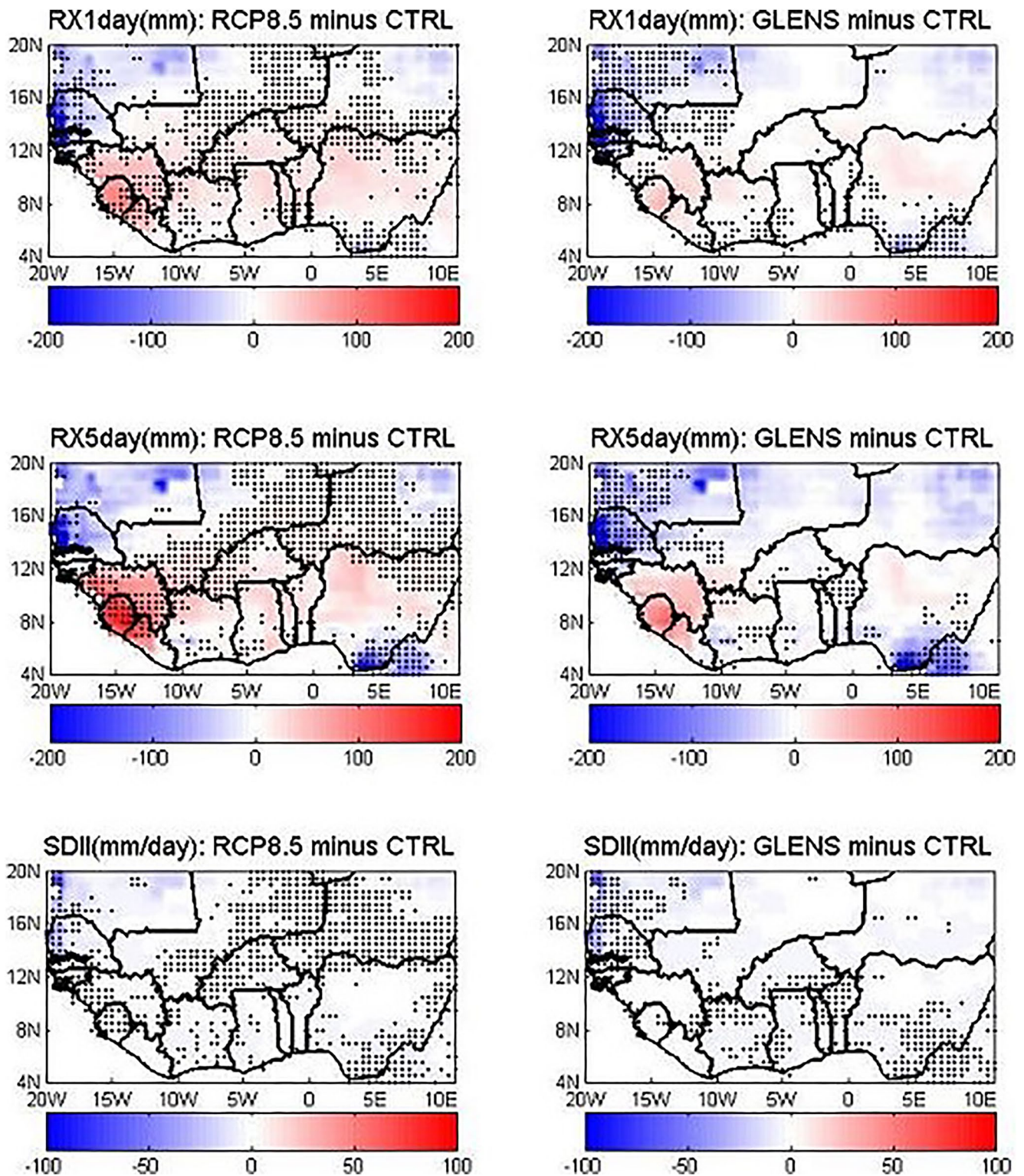
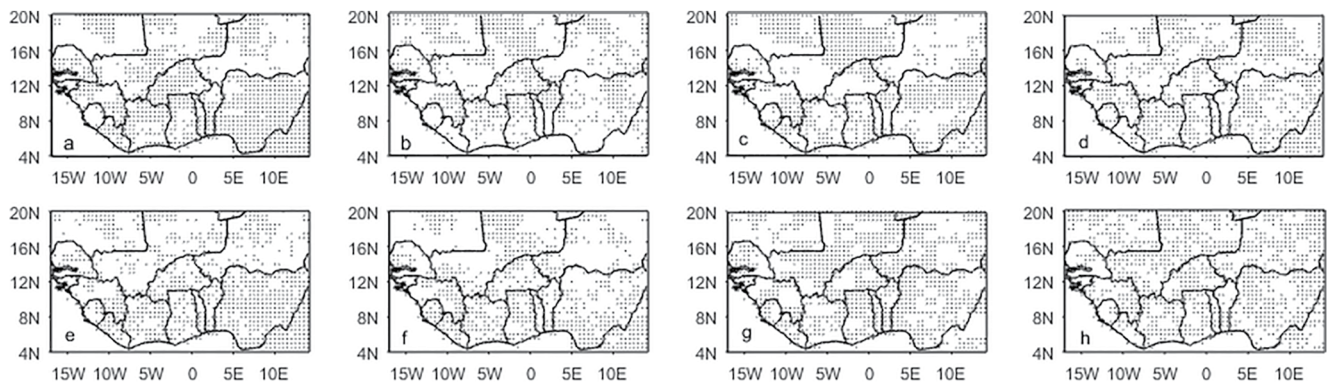**Figure 7.** Changes in Max 1-day precipitation amount (Line 1), Max 5-days precipitation amount (Line 2) and Simple daily intensity index (Line 3) over the period 2070–2090 compared to the control period (2010–2030) under representative concentration pathway 8.5 and Geoengineering Large Ensemble simulations. Hatching indicates regions where changes are statistically significant at the 95% confidence level.
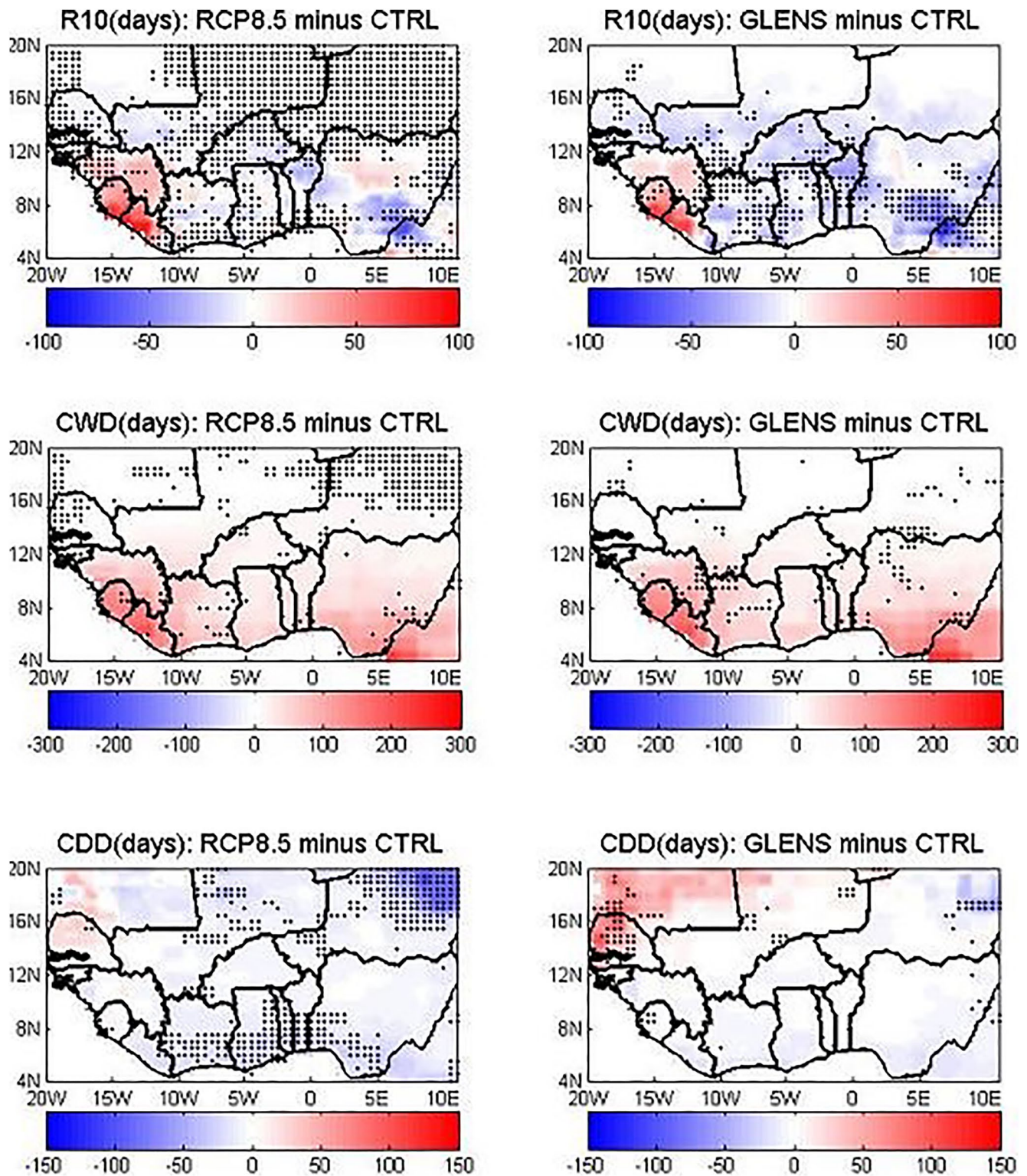
Figure 8. Changes in the Number of heavy precipitation days (R10) (Line 1), the number of Consecutive wet days (Line 2), the number of Consecutive dry days (Line 3) over the period 2070–2090 compared to the control period (2010–2030) under representative concentration pathway 8.5 and Geoengineering Large Ensemble simulations. Hatching indicates regions where changes are statistically significant at the 95% confidence level.
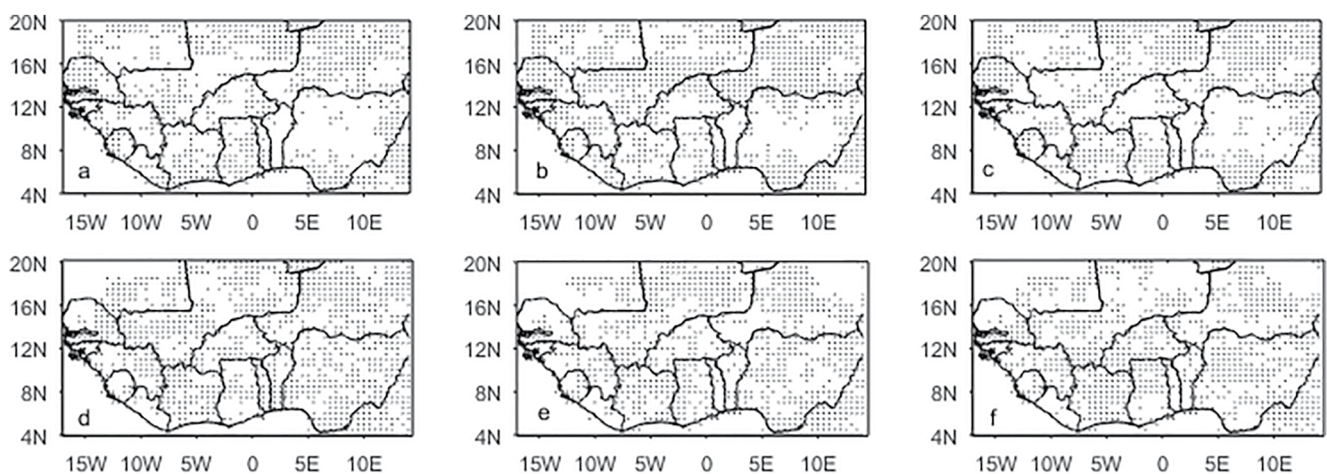
Figure 9. Granger causality between global mean sea surface temperature and extreme precipitation indices (a) for P, (b) for Max 1-day precipitation amount, (c) for Max 5-day precipitation amount, (d) for Simple daily intensity index, (e) for R10, (f) for R20, (g) for consecutive dry days and (h) for Consecutive wet days under Geoengineering Large Ensemble simulations over the period 2070–2090. Hatching indicates regions where Granger causal relationship are statistically significant at the 95% confidence level.

oceanic basins. It could also be that the variability in these indices is driven by local scale than large-scale SST variability (Atiah et al., 2020).

To assess which parts of oceans basin have caused change in extreme precipitation indices in West Africa, NINO3.4, IOD and AMO indices, are used for Granger causality with extreme precipitations indices. Figure 10 shows the causal relationships between SDII respectively with AMO, IOD, and NINO3.4 indices. Under RCP8.5 scenario, significant Granger causal relationships are found between SDII and SST indices. These significant causal relationships are scattered throughout West Africa with NINO3.4, AMO, and IOD, except in in many areas of Nigeria, Benin, Senegal and Mauritania. Under GLENS, we notice that the areas, which showed non significant causal relationship under RCP8.5, depicted now significant causal relationships. The same pattern of causality is found between the others intensity indices (RX1day and RX5day (Figure 11)), frequency indices (R10 (Figure 12) and R20).

Figure 13 presents the causal relationships between annual precipitation and SST indices. Under RCP8.5, non-significant causal relationship were found between annual precipitation and AMO indices in West Africa, except in southern of Nigeria, southern Malia, and northern Senegal. Under GLENS, significant causal relationships were observed in most West Africa countries. Under RCP8.5, more non-significant causal relationship were observed between annual precipitation and respectively NINO3.4 and IOD in West Africa in comparison to the

Figure 10. Granger causality between Simple daily intensity index and sea surface temperature indices under both representative concentration pathway 8.5 (a) for Atlantic Multidecadal Oscillation (AMO), (b) for Indian Ocean Dipole (IOD), (c) for NINO3.4 and Geoengineering Large Ensemble simulations scenarios (d) for AMO, (e) for IOD, (f) for NINO3.4 over the period 2070–2090. Hatching indicates regions where Granger causal relationship are statistically significant at the 95% confidence level.
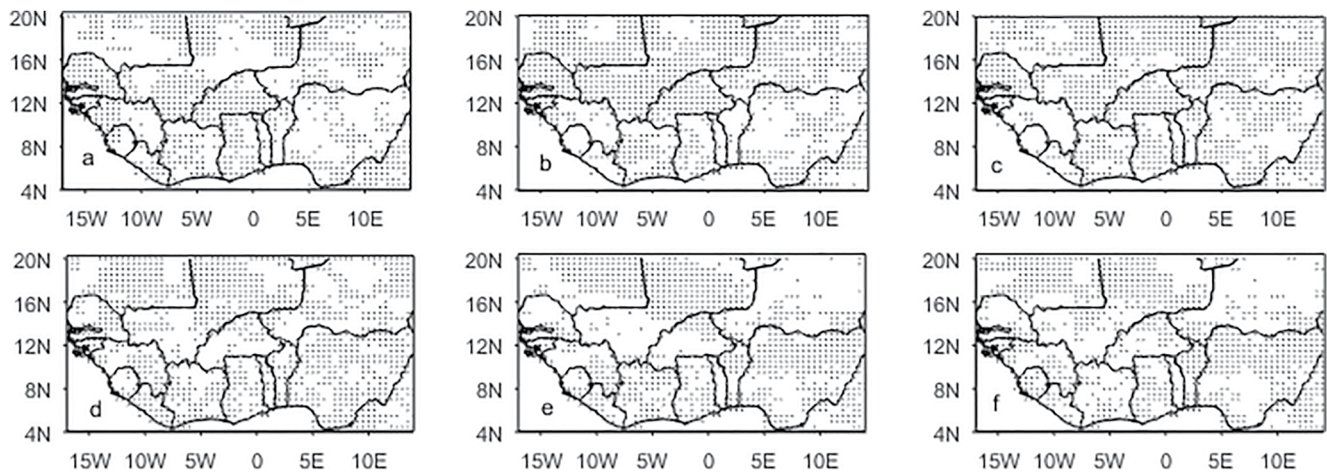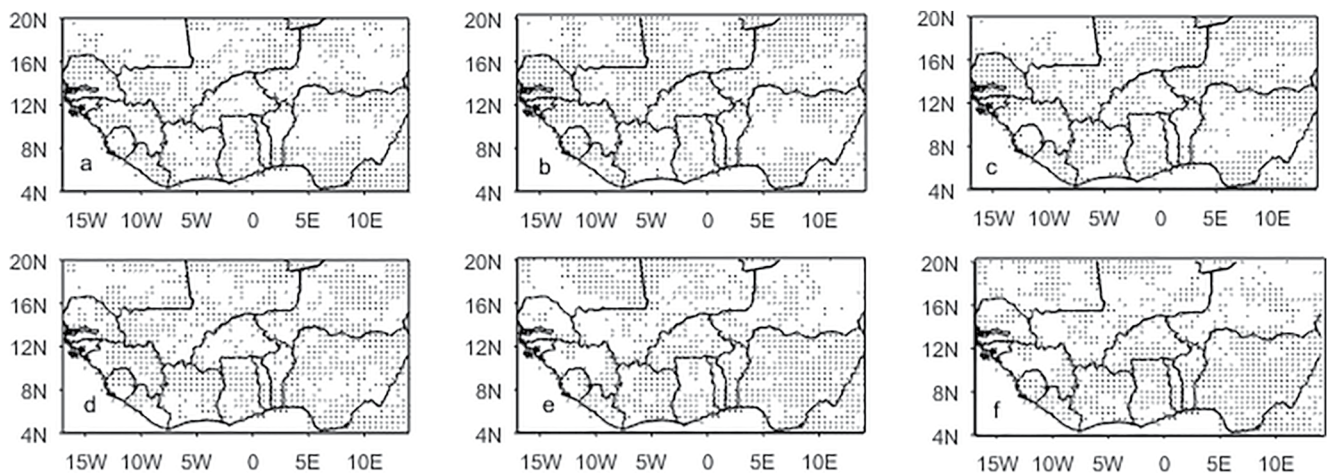
Figure 11. Granger causality between RX5day and sea surface temperature indices under both representative concentration pathway 8.5 (a) for Atlantic Multidecadal Oscillation (AMO), (b) for Indian Ocean Dipole (IOD), (c) for NINO3.4 and Geoengineering Large Ensemble simulations scenarios (d) for AMO, (e) for IOD, (f) for NINO3.4 over the period 2070–2090. Hatching indicates regions where Granger causal relationship are statistically significant at the 95% confidence level.

results under GLENS. Almost the same pattern of significant causal relationships were found between CDD and SST under RCP8.5 and GLENS simulations (Figure 14). These findings are consistent with several works (Atiah et al., 2020; Diatta et al., 2020, etc.) which found that changes in extreme precipitation indices in West Africa can be linked to changes in AMO, NINO3.4, and IOD indices.

3.5. Mechanism of Changes in Extreme Precipitation Under GLENS

Figure 15 shows the spatial pattern of annual surface specific humidity and 957 hPa wind field for the CRTL period and changes (relative to the CRTL period) in mean annual surface specific humidity and 957 hPa wind field under RCP8.5 and GLENS scenarios. Under RCP8.5, near surface specific humidity increases related to CRTL period. This increase of near surface specific humidity contributes to intensify climatological precipitation pattern under global warming (Da-Allada et al., 2020). Under GLENS, near surface specific humidity slightly decrease related to the CRTL period. Contrary to RCP8.5, change in near surface specific humidity is small under GLENS and it could make negligible contribution to rainfall decrease. General circulation could therefore play a key role in the decrease of precipitation under GLENS. We found that under GLENS there is a weakening of the winds coming from the oceanic basin (Figure 15). As the solar radiation varies with the season and land would

Figure 12. Granger causality between R10 and sea surface temperature indices under both representative concentration pathway 8.5 (a) for Atlantic Multidecadal Oscillation (AMO), (b) for Indian Ocean Dipole (IOD), (c) for NINO3.4 and Geoengineering Large Ensemble simulations scenarios (d) for AMO, (e) for IOD, (f) for NINO3.4 over the period 2070–2090. Hatching indicates regions where Granger causal relationship are statistically significant at the 95% confidence level.
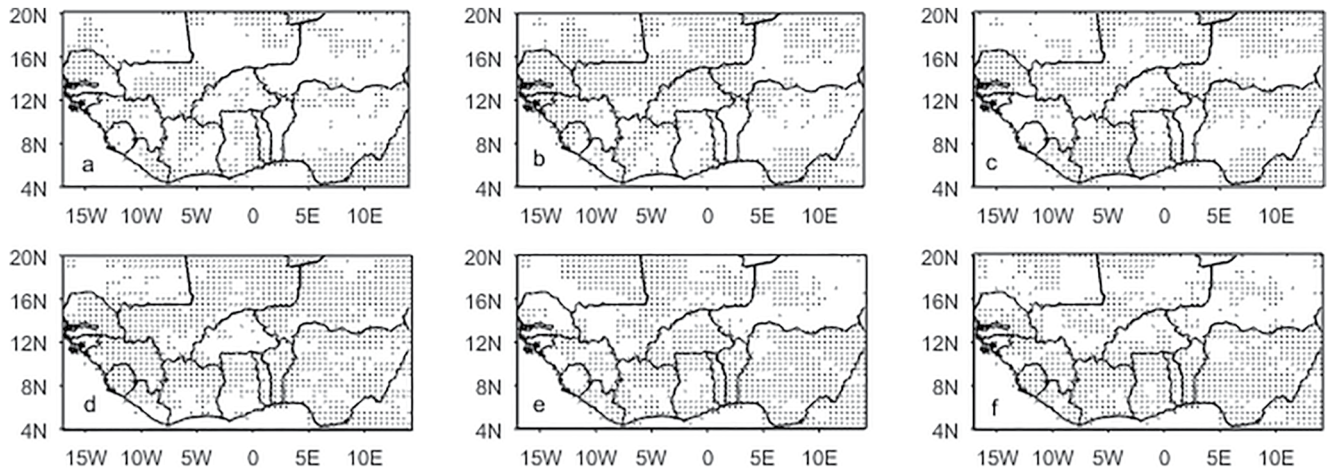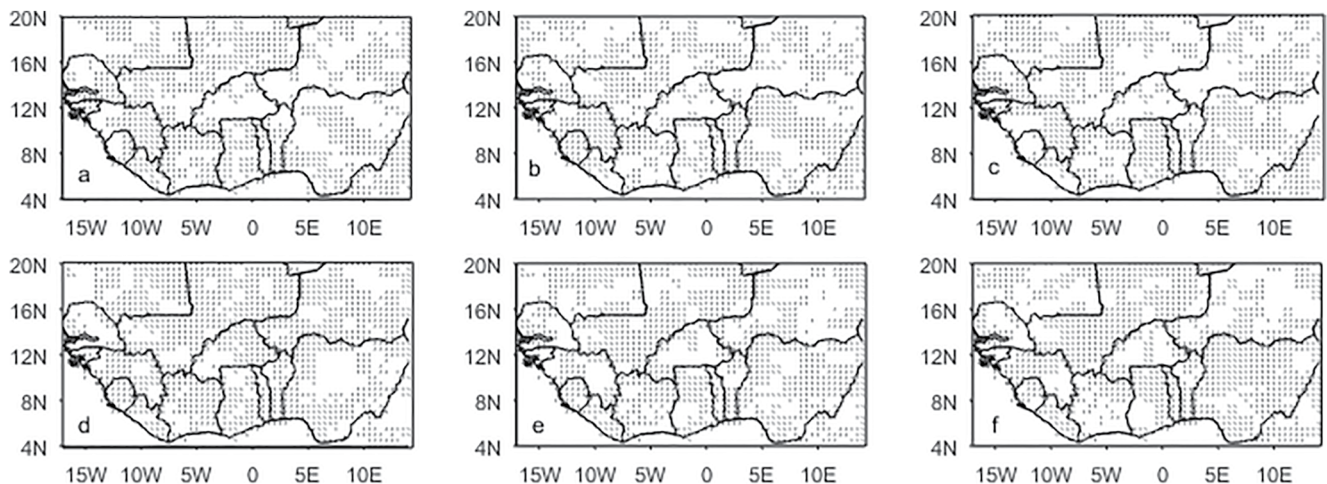
Figure 13. Granger causality between annual precipitation and sea surface temperature indices under both representative concentration pathway 8.5 (a) for Atlantic Multidecadal Oscillation (AMO), (b) for Indian Ocean Dipole (IOD), (c) for NINO3.4 and Geoengineering Large Ensemble simulations scenarios (d) for AMO, (e) for IOD, (f) for NINO3.4 over the period 2070–2090. Hatching indicates regions where Granger causal relationship are statistically significant at the 95% confidence level.

warm or cool faster than ocean (due to the heat capacity of water which is more important than that of the land), the low-level land-sea thermal contrast is strongly influenced by solar radiation (Liu et al., 2019). The reduction of land-sea thermal contrast in GLENS leads to weak monsoon winds [as also found in Da-Allada et al. (2020)] and a slight southward shift of the ITCZ (by around 0.18°) relative to the baseline period (Cheng et al., 2019). In summary, under GLENS, decrease in precipitation are largely driven by weakened monsoon circulation due to the reduce of land-sea thermal contrast in the lower troposphere.

4. Discussion

This paper provides an overview of the response of SAG on climate over West African countries using the CESM1 (WACCM) model from the GLENS experiment. In the GLENS simulation, sulfur is injected at four latitudes in the stratosphere with the aim to maintain global mean surface temperatures at 2020 values. We compare the possible impacts of this experiment and the RCP8.5 scenario in the late 21st century (2070–2090) to a CRTL period (2010–2030) of the RCP8.5 scenario. ISIMIP bias correction method has been used to bias correct precipitation and temperatures data before computing the extreme indices. Previous studies have also shown that

Figure 14. Granger causality between consecutive dry days and sea surface temperature indices under both representative concentration pathway 8.5 (a) for Atlantic Multidecadal Oscillation (AMO), (b) for Indian Ocean Dipole (IOD), (c) for NINO3.4 and Geoengineering Large Ensemble simulations scenarios (d) for AMO, (e) for IOD, (f) for NINO3.4 over the period 2070–2090. Hatching indicates regions where Granger causal relationship are statistically significant at the 95% confidence level.
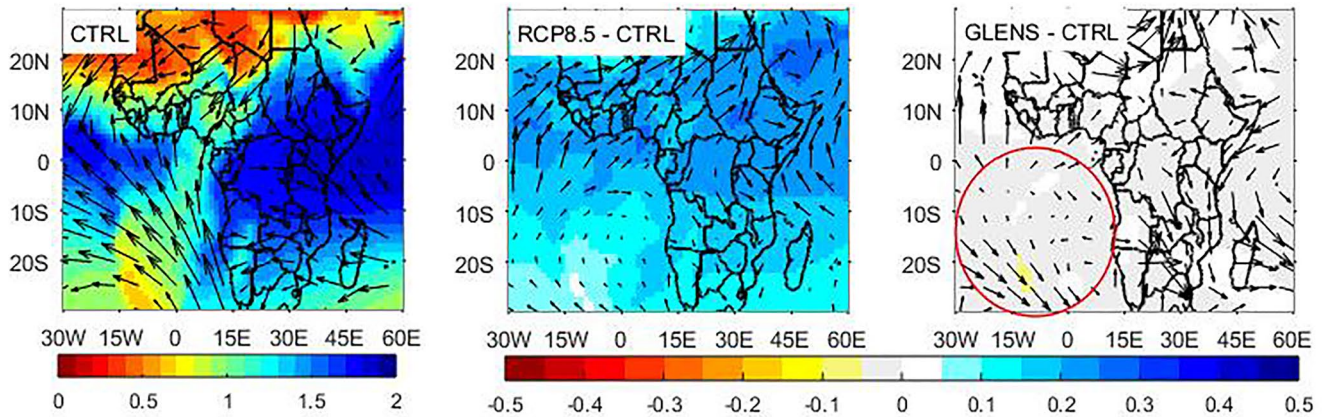
Figure 15. Spatial pattern of annual surface specific humidity (color shading) and 957 hPa wind field (vectors) for the control period and changes (relative to the control) in mean annual surface specific humidity (color shading) and 957 hPa wind field (vectors) under representative concentration pathway 8.5 and Geoengineering Large Ensemble simulations. The units are 10^{-2} kg kg m s^{-1} for specific humidity.

the ISIMIP method is one of the best bias correction method (Obada et al., 2016; Wörner et al., 2019). ETCCDI extreme temperature and precipitation indices are used as metrics to evaluate the potential impacts of GLENS experiment and RCP8.5 scenario, in terms of change, on climate relative to the CRTL period.

The results show a statistically significant increase of minimum, maximum and mean temperature under RCP8.5 compared to the CRTL period, while under GLENS we found mostly non significant decrease compared to the CRTL period. We also found that cold extreme temperature indices (here Cold days, Cold nights, and CSDI) would statistically significantly decrease under RCP8.5 scenario compared to the CRTL period, while under GLENS simulations these indices are mostly no significant increase compared to the CRTL period. The robust increase in CSDI is found over the tropical oceans with more than 50 days per year over large regions (Ji et al., 2018), indicating that the region is sensitive to reduced solar radiation. With regard to hot extreme temperature indices, the results indicate that GLENS experiment reduces these indices compared to the results obtained with RCP8.5 scenario. Shi et al. (2018) showed that the hot extreme temperature indices generally increase under the different RCPs scenarios. In general, SAG would maintain future (2070–2090) surface mean temperature and extreme temperature indices closer to CRTL period (2010–2030). Pinto et al. (2020) also found similar results over Africa. The previous results imply that GLENS experiment in future could lead to climate that is closer to the CRTL period in West Africa.

In the present study, we found that GLENS simulations increase annual precipitation relative to CRTL period. However, the annual precipitation under GLENS simulations is less than the annual precipitation obtained under RCP8.5 scenario for many West African countries. This finding is also confirmed by Simpson et al. (2019) who found that GLENS results in a reduction in precipitation relative to RCP8.5 scenario over some regions and seasons with climatologically high precipitation in Africa. Pinto et al. (2020) also found a reduction in precipitation under GLENS simulations relative to RCP8.5 scenario in Central and West Africa, and they suggested that it may be the result of a reduced impact on the Hadley circulation of global warming brought about by SAG. The reduction in precipitation under the SAG compared to RCP8.5 in West African Summer Monsoon is mainly caused by changes in the dynamic processes (monsoon circulation) (Da-Allada et al., 2020).

Under SAG, extreme precipitation intensity decreases in the sahelian region, while it increases in the Gulf of Guinea compared to the CRTL period. The same pattern is found under RCP8.5 compared to the CRTL period. However, we found that SAG generally offsets the increase in RX1day, RX5day, and SDII seen in RCP8.5 scenario. The decrease in RX5days is in line with the findings of Curry et al. (2014) and Ji et al. (2018). In fact, Curry et al. (2014) reported a decrease in RX5days under G1 simulation compared to piControl simulation using a GeoMIP multi-model ensemble while, Ji et al. (2018) reported a decrease in this index under G4 simulation (GeoMIP) compared to the RCP4.5 scenario.

When assessing change in precipitation frequency indices, we found that under SAG, there are no significant changes in CDD and CWD compared to the CRTL period. These results are in line with the findings of Curry

et al. (2014), Dosio et al. (2019), Ji et al. (2018), and Pinto et al. (2020) . However, for the other frequency indices (R10, R20), the results show a statistically significant decrease in these indices under GLENS experiment related to CRTL period in Gulf of Guinea region, except Guinea, Sierra Leone, Liberia where statistically significant increase were found.

The reduction in precipitation relative to CRTL period cannot be directly linked to reductions in water availability or increases in droughts as reduction in temperature also reduces evaporation (Da-Allada et al., 2020; Pinto et al., 2020). However, the decrease in RX1day and RX5days precipitation amount and in frequency of R10, R20 under SAG could have a positive impact on flash flood occurrences and its socio-economic impact in this region.

Projected changes in temperature and rainfall under RCP8.5 scenario would likely increase diseases and the occurrence of extreme water stress (Cashman et al., 2010; Nelson et al., 2009; Pulwarty et al., 2010; Simpson et al., 2010). However, under SAG, we would notice less extreme temperature and precipitation than in a world without SAG as also showed by Pinto et al. (2020). Granger causality test between extreme precipitation indices and SST indices indicate that changes in extreme precipitation indices in West Africa is linked to changes in SST. The decrease in extreme precipitation under GLENS could be explained by the decrease in near surface specific humidity over tropical region due to the decrease in SST over this region. The decrease in extreme precipitation indices under GLENS simulations would also be caused by the reduction of the low-level land-sea thermal contrast (Da-Allada et al., 2020) and this reduction of land-sea thermal contrast leads to weak monsoon winds and a slight southward shift of the ITCZ (by around 0.18°) relative to the baseline (Cheng et al., 2019).

5. Conclusions

The main contribution of this paper was to assess, first, the changes in extreme precipitation and temperature and second, the link between SST anomalies and extreme precipitation in West Africa under a high greenhouse gas scenario and using SAG to keep global surface temperatures at present day values. The ISIMIP bias correction method used in the present study allows reducing the large differences between observations data and GLENS simulations. Under SAG, the results showed a decrease in the minimum, maximum and mean temperatures and in the hot extremes temperature indices (TX90p, TN90p, TR, SU, WSDI) compared to the results obtained with RCP8.5 scenarios over the period 2070–2097. In agreement with previous studies (e.g., Ji et al., 2018), our results showed a non statistically increase in the cold extreme indices under GLENS simulations relative to the CRTL period.

Changes in annual and extreme precipitations are expected to have an impact on water availability, which is essential in this region, and need to be investigated in more detail. GLENS showed a decrease in the precipitation intensity indices (RX1day, RX5day, and SDII) compared to the CRTL period. For the precipitation frequency indices, a statistically significant decrease (in R10 and R20) and a mix of slight non statistically significant decrease and increase (in CWD and CDD) are simulated in the study area. Under SAG, the changes in extremes temperature indices were found to be more effectively reduced compared to extremes precipitation indices. The changes in extreme precipitation indices are linked with changes in AMO, NINO3.4, and IOD and these changes in extreme precipitation are driven by change in near surface specific humidty and atmospheric circulation.

Data Availability Statement

The data used in this study are available to the community via the Earth System Grid (see information at www.cesm.ucar.edu/projects/community-projects/GLENS/; Tilmes, Ritcher, Mills, et al., 2018).

References

Ammann, C. M., Washington, W. M., Meehl, G. A., Buja, L., & Teng, H. (2010). Climate engineering through artificial enhancement of natural forcings: Magnitudes and implied consequences. *Journal of Geophysical Research*, *115*(D22), D22109. https://doi.org/10.1029/2009jd012878

Atiah, W. A., Tsidu, G. M., Amekudzi, L. K., & Yorke, C. (2020). Trends and interannual variability of extreme rainfall indices over Ghana, West Africa. *Theoretical and Applied Climatology*, *140*(3), 1393–1407. https://doi.org/10.1007/s00704-020-03114-6

Bala, G., Duffy, P. B., & Taylor, K. E. (2008). Impact of geoengineering schemes on the global hydrological cycle. *Proceedings of the National Academy of Sciences of the United States of America*, *105*(22), 7664–7669. https://doi.org/10.1073/pnas.0711648105

Barnston, A. G., & Tippett, M. K. (2013). Predictions of NINO3.4 SST in CFSv1 and CFSv2: A diagnostic comparison. *Climate Dynamics*, *41*(5–6), 1615–1633. https://doi.org/10.1007/s00382-013-1845-2

Caldeira, K., & Wood, L. (2008). Global and Arctic climate engineering: Numerical model studies. *Philosophical Transactions of the Royal Society of London*, *366*(1882), 4039–4056. https://doi.org/10.1098/rsta.2008.0132

Camberlin, P., Janicot, S., & Poccard, I. (2001). Seasonality and atmospheric dynamics of the teleconnection between African rainfall and tropical sea-surface temperature: Atlantic vs. ENSO. *International Journal of Climatology*, *21*(8), 973–1005. https://doi.org/10.1002/joc.673

Cashman, A., Nurse, L., & Charlery, J. (2010). "Climate change in the Caribbean: The water management implications." *The Journal of Environment and Development*, *19*(1), 42–67. https://doi.org/10.1177/1070496509347088

Chang, C.-P., Zhang, Y.-S., & Li, T. (2000). Interannual and interdecadal variations of the East Asian summer monsoon and tropical Pacific SSTs, part II: Meridional structure of the monsoon. *Journal of Climate*, *13*(24), 4326–4340. https://doi.org/10.1175/1520-0442(2000)013<4326:iaivot>2.0.co;2

Cheng, W., MacMartin, D. G., Dagon, K., Kravitz, B., Tilmes, S., Richter, J. H., et al. (2019). Soil moisture and other hydrological changes in a stratospheric aerosol geoengineering large ensemble. *Journal of Geophysical Research: Atmospheres*, *124*(23), 12773–12793. https://doi.org/10.1029/2018JD030237

Crutzen, P. J. (2006). Albedo enhancement by stratospheric sulfur injections: A contribution to resolve a policy dilemma? *Climatic Change*, *77*(3–4), 211–220. https://doi.org/10.1007/s10584-006-9101-y

Curry, C. L., Sillmann, J., Bronaugh, D., Alterskjaer, K., Cole, J. N., Ji, D., et al. (2014). A multimodel examination of climate extremes in an idealized geoengineering experiment. *Journal of Geophysical Research: Atmospheres*, *119*(7), 3900–3923. https://doi.org/10.1002/2013JD020648

Da-Allada, C. Y., Baloïtcha, E., Alamou, E. A., Awo, F. M., Banou, F., Pomalegni, Y., et al. (2020). Changes in West African summer monsoon precipitation under stratospheric aerosol geoengineering. *Earth's Future*, *8*(7), e2020EF001595. https://doi.org/10.1029/2020EF001595

Diatta, S., Diedhiou, C. W., Dione, D. M., & Sambou, S. (2020). Spatial variation and trend of extreme precipitation in West Africa and teleconnections with remote indices. *Atmosphere*, *11*(9), 999. https://doi.org/10.3390/atmos11090999

Diatta, S., & Fink, H. A. (2014). Statistical relationship between remote climate indices and West African monsoon variability. *International Journal of Climatology*, *34*(12), 3348–3367. https://doi.org/10.1002/joc.3912

Dosio, A., Jones, R. G., Jack, C., Lennard, C., Nikulin, G., & Hewitson, B. (2019). What can we know about future precipitation in Africa? Robustness, significance and added value of projections from a large ensemble of regional climate models. *Climate Dynamics*, *1*, 26. https://doi.org/10.1007/s00382-019-04900-3

Enfield, D. B., Mestas-Nuñez, A. M., & Trimble, P. J. (2001). The Atlantic multidecadal oscillation and its relation to rainfall and river flows in the continental US. *Geophysical Research Letters*, *28*(10), 2077–2080. https://doi.org/10.1029/2000gl012745

Gao, T., Wang, H. J., & Zhou, T. (2017). Changes of extreme precipitation and nonlinear influence of climate variables over monsoon region in China. *Atmospheric Research*, *197*, 379–389. https://doi.org/10.1016/j.atmosres.2017.07.017

Giannini, A., Saravanan, R., & Chang, P. (2003). Oceanic forcing of Sahel rainfall on interannual to interdecadal time scales. *Science*, *302*(5647), 1027–1030. https://doi.org/10.1126/science.1089357

Govindasamy, B., & Caldeira, K. (2000). Geoengineering Earth's radiation balance to mitigate CO_2-induced climate change. *Geophysical Research Letters*, *27*(14), 2141–2144. https://doi.org/10.1029/1999gl006086

Govindasamy, B., Caldeira, K., & Duffy, P. (2003). Geoengineering Earth's radiation balance to mitigate climate change from a quadrupling of CO_2. *Global and Planetary Change*, *37*(1–2), 157–168. https://doi.org/10.1016/S0921-8181(02)00195-9

Granger, C. W. J. (1969). Investigating causal relations by econometric models and cross-spectral methods. *Econometrica*, *37*(3), 424–438. https://doi.org/10.2307/1912791

Hempel, S., Frieler, K., Warszawski, L., Schewe, J., & Piontek, F. (2013). A trend-preserving bias correction - The ISI-MIP approach. *Earth System Dynamics*, *4*, 219–236. https://doi.org/10.5194/esd-4-219-2013

Ji, D., Fang, S., Curry, C. L., Kashimura, H., Shingo, W., Cole, J. N. S., et al. (2018). Extreme temperature and precipitation response to solar dimming and stratospheric aerosol geoengineering. *Atmospheric Chemistry and Physics Discussions*, *18*(14), 10133–10156. https://doi.org/10.5194/acp-18-10133-2018

Kalidindi, S., Bala, G., Modak, A., & Caldeira, K. (2015). Modeling of solar radiation management: A comparison of simulations using reduced solar constant and stratospheric sulphate aerosols. *Climate Dynamics*, *44*(9), 2909–2925. https://doi.org/10.1007/s00382-014-2240-3

Kravitz, B., Caldeira, K., Boucher, O., Robock, A., Rasch, P. J., Alterskjær, K., et al. (2013). Climate model response from the geoengineering model Intercomparison project (GeoMIP). *Journal of Geophysical Research: Atmospheres*, *118*(15), 8320–8332. https://doi.org/10.1002/jgrd.50646

Kravitz, B., Douglas, G., MacMartin, M. J., Mills, J. H. R., Tilmes, S., Lamarque, J. F., et al. (2017). First simulations of designing stratospheric sulfate aerosol geoengineering to meet multiple simultaneous climate objectives. *Journal of Geophysical Research: Atmospheres*, *122*(24), 12616–12634. https://doi.org/10.1002/2017JD026874

Kravitz, B., Rasch, P. J., Forster, P. M., Andrews, T., Cole, J. N., Irvine, P. J., et al. (2013). An energetic perspective on hydrological cycle changes in the Geoengineering Model Intercomparison Project. *Journal of Geophysical Research: Atmospheres*, *118*(23), 13087–13102. https://doi.org/10.1002/2013JD020502

Launder, B., & Thompson, J. (Eds.), (2009). *Geo-engineering climate change: Environmental necessity or Pandora's box?* Cambridge Univ. Press.

Liu, Y., Cai, W., Sun, C., Song, H., Cobb, K. M., Li, J., et al. (2019). Anthropogenic aerosols cause recent pronounced weakening of Asian Summer Monsoon relative to last four centuries. *Geophysical Research Letters*, *46*(10), 5469–5479. https://doi.org/10.1029/2019GL082497

Ly, M., Traore, B. S., Alhassane, A., & Sarr, B. (2013). Evolution of some observed climate extremes in the West African Sahel. *Weather and Climate Extremes*, *1*, 19–25. https://doi.org/10.1016/j.wace.2013.07.005

McCusker, K. E., Battisti, D. S., & Bitz, C. M. (2012). The climate response to stratospheric sulfate injections and implications for addressing climate emergencies. *Journal of Climate*, *25*(9), 3096–3116. https://doi.org/10.1175/JCLI-D-11-00183.1

Mills, M. J., Richter, J. H., Tilmes, S., Kravitz, B., MacMartin, D. G., Glanville, A. A., et al. (2017). Radiative and chemical response to interactive stratospheric sulfate aerosols in fully coupled CESM1 (WACCM). *Journal of Geophysical Research: Atmospheres*, *122*(23), 13–61. https://doi.org/10.1002/2017JD027006

Nelson, G. C., Rosegrant, R. W., Koo, J., Robertson, R., Sulser, T., Zhu, T., et al. (2009). *Climate change: Impact on agriculture and costs of adaptation*. International Food Policy Research Institute. https://doi.org/10.2499/0896295354

Nicholson, S. E. (2013). The West African Sahel: A review of recent studies on the rainfall regime and its interannual variability. *ISRN Meteorology*, *2013*, 453521. https://doi.org/10.1155/2013/453521

Niemeier, U., Schmidt, H., Alterskjær, K., & Kristjánsson, J. E. (2013). Solar irradiance reduction via climate engineering: Impact of different techniques on the energy balance and the hydrological cycle. *Journal of Geophysical Research: Atmospheres*, *118*(21), 11905–11917. https://doi.org/10.1002/2013JD020445

Obada, E., Alamou, A. E., Zandagba, E. J., Biao, I. E., Chabi, A., & Afouda, A. (2016). Comparative study of seven bias correction methods applied to three Regional Climate Models in Mekrou catchment (Benin, West Africa). *International Journal of Current Engineering and Technology*, *6*(5), 1831–1840.

Onojeghuo, A. R., Balzter, H., & Monks, P. S. (2017). Tropospheric NO$_2$ concentrations over West Africa are influenced by climate zone and soil moisture variability. *Atmospheric Chemistry and Physics Discussions*, 1–25. https://doi.org/10.5194/acp-2016-1128-AC1

Pinto, I., Jack, C., Lennard, C., Tilmes, S., & Odoulami, R. C. (2020). *Africa's climate response to solar radiation management with stratospheric aerosol*. American Geophysical Union. https://doi.org/10.1029/2019GL086047

Pulwarty, R., Nurse, L., & Trotz, U. O. (2010). Caribbean islands in a changing climate. *Environment: Science and Policy for Sustainable Development*, *52*(6), 16–27. https://doi.org/10.1080/00139157.2010.522460

Razavi, T., Switzman, H., Arain, A., & Coulibaly, P. (2016). Regional climate change trends and uncertainty analysis using extreme indices: A case study of Hamilton, Canada. *Climate Risk Management*, *13*, 43–63. https://doi.org/10.1016/j.crm.2016.06.002

Ricke, K. L., Morgan, M. G., & Allen, M. R. (2010). Regional climate response to solar- radiation management. *Nature Geoscience*, *3*(8), 537–541. https://doi.org/10.1038/ngeo915

Schmidt, H., Alterskjær, K., Bou Karam, D., Boucher, O., Jones, A., & Kristjánsson, J. E. (2012). Solar irradiance reduction to counteract radiative forcing from a quadrupling of CO$_2$: Climate responses simulated by four Earth system models. *Earth System Dynamics*, *3*(1), 63–78. https://doi.org/10.5194/esd-3-63-2012

Shi, C., Jiang, Z. H., Chen, W. L., & Li, L. (2018). Changes in temperature extremes over China under 1.5°C and 2°C global warming targets. *Advances in Climate Change Research*, *9*(2), 120–129. https://doi.org/10.1016/j.accre.2017.11.003ff.ffhal-02414708

Simpson, I. R., Tilmes, S., Richter, J. H., Kravitz, B., MacMartin, D. G., Mills, M. J., et al. (2019). The regional hydroclimate response to stratospheric sulphate geoengineering and the role of stratospheric heating. *Journal of Geophysical Research: Atmospheres*, *124*(23), 12587–12616. https://doi.org/10.1029/2019jd031093

Simpson, M. C., Scott, D., Harrison, M., et al. (2010). *Quantification and magnitude of losses and damages resulting from the impacts of climate change: Modelling the transformational impacts and costs of sea level rise in the Caribbean (full document)*. Barbados, West Indies: United Nations Development Programme (UNDP).

Sultan, B., & Gaetani, M. (2016). Agriculture in West Africa in the twenty-first century: Climate change and impacts scenarios, and potential for adaptation. *Frontiers of Plant Science*, *7*, 1262. https://doi.org/10.3389/fpls.2016.01262

Sylla, M. B., Diallo, I., & Pal, J. S. (2013). West African monsoon in state-of-the-science regional climate models. *Climate Variability—Regional and Thematic Patterns*, *10*(55140), 1805–1817. https://doi.org/10.5772/55140

Sylla, M. B., Nikiema, P. M., Gibba, P., Kebe, I., & Klutse, N. A. B. (2016). Climate change over West Africa: Recent trends and future projections. In J. A. Yaro & J. Hesselberg (Eds.), *Adaption to climate change and variability in rural West Africa*, 25–40. Springer. https://doi.org/10.1007/978-3-319-31499-0_3

Tilmes, S., Fasullo, J., Lamarque, J. F., Marsh, D. R., Mills, M., Alterskjær, K., et al. (2013). The hydrological impact of geoengineering in the Geoengineering Model Intercomparison Project (GeoMIP). *Journal of Geophysical Research: Atmospheres*, *118*(19), 11036–11058. https://doi.org/10.1002/jgrd.50868

Tilmes, S., Richter, J. H., Kravitz, B., MacMartin, D. G., Mills, M. J., & Simpson, I. R. (2018). CESM1 (WACCM) stratospheric aerosol geoengineering large ensemble project. *Bulletin of the American Meteorological Society*, *99*(11), 2361–2371. https://doi.org/10.1175/BAMS-D-17-0267.1

Tilmes, S., Richter, J. H., Mills, M., Kravitz, B., Douglas, G., & MacMartin, G. D. (2018). Stratospheric aerosol geoengineering large ensemble [Dataset]. UCAR/NCAR Earth System Grid. https://doi.org/10.5065/D6JH3JXX

Vinayachandran, P. N., Murty, V. S. N., & Babu, V. R. (2002). Observations of barrier layer formation in the Bay of Bengal during summer monsoon. *Journal of Geophysical Research*, *107*(C12), 8018. https://doi.org/10.1029/2001JC000831

Vizy, E. K., & Cook, K. H. (2001). Mechanisms by which Gulf of Guinea and eastern North Atlantic sea surface temperature anomalies can influence African rainfall. *Journal of Climate*, *14*(5), 795–821. https://doi.org/10.1175/1520-0442(2001)014<0795:mbwgog>2.0.co;2

Wörner, V., Kreye, P., & Meon, G. (2019). Effects of bias-correcting climate model data on the projection of future changes in high flows. *Hydrology*, *6*(2), 46. https://doi.org/10.3390/hydrology6020046

Zhang, X., Alexander, L., Hegerl, G. C., Jones, P., Tank, A. K., Peterson, T. C., et al. (2011). Indices for monitoring changes in extremes based on daily temperature and precipitation data. *WIREs Climate Change*, *2*(6), 851–870. https://doi.org/10.1002/wcc.147